We are IntechOpen,
the world's leading publisher of
Open Access books
Built by scientists, for scientists

6,900
Open access books available

186,000
International authors and editors

200M
Downloads

Our authors are among the

154
Countries delivered to

TOP 1%
most cited scientists

12.2%
Contributors from top 500 universities

CLARIVATE ANALYTICS
BOOK CITATION INDEX
INDEXED

WEB OF SCIENCE™

Selection of our books indexed in the Book Citation Index
in Web of Science™ Core Collection (BKCI)

Interested in publishing with us?
Contact book.department@intechopen.com

Wading into a Theoretical Model for Parkinson's Disease

Diana W. Verzi
San Diego State University-Imperial Valley Campus
USA

1. Introduction

While a lot of work has been done on theoretical models for learning and memory, with implications for Alzheimer's disease, little mathematical modeling has been offered for Parkinson's disease, a neurodegenerative disorder of the basal ganglia. The disease is characterized by progressive loss of dopaminergic neurons in the substantia nigra pars compacta, and movement disorders are associated with abnormalities in electrical activity within the substantia nigra pars reticulata. (Brown et al., 1982; Guatteo et al., 2005)

An early study implicated a thermoregulatory role for dopamine receptors in the substantia nigra, but the functional significance of this location in temperature regulation remained to be elucidated (Brown et al., 1982). More recently, changes in temperature of up to several degrees have been reported in different brain regions during various behaviors or in response to environmental stimuli. This lead to the conclusion that temperature-gated TRPV3 and TRPV4 cationic channels are expressed in nigral dopaminergic neurons, and they are active in brain slices at near physiological temperatures, affecting neuronal excitability and calcium homeostasis (Guatteo et al., 2005).

A reduction in the frequency of neuron firing within the striata nigra has been linked to a loss of dopaminergic neurons. A study of spontaneous neuron firing, cell membrane potential and currents, and intracellular calcium levels in dopaminergic neurons of the rat substantia nigra was conducted under varying temperature controls (Guatteo et al., 2005). Cooling evoked slowing of firing, cell membrane hyperpolarization, increase in cell input resistance, and outward current under voltage clamp, along with a decrease in intracellular Ca2+. Warming induced an increase in firing frequency, a decrease in input resistance, an inward current and a rise in Ca2+. Neurons within the globus pallidus and substantia nigra form a functional network that ideally resonates around *70Hz* for normal voluntary movement. However, this network has been observed to oscillate at frequencies below 30*Hz* in Parkinson patients, and these oscillations are believed to disrupt normal motor function (Basu et al., 2010).

Post-morten cortices from Parkinson patients exhibit biochemical and physical alterations within dendritic arbors (Patt et al., 1991; Stephens et al., 2005), and it has been suggested that activity-dependent intraspine calcium may regulate dendritic morphology, affecting the synaptic connection between neurons (Stephens et al., 2005). One theory holds that sporadic Parkinson's involves a breakdown of the mitochondria (Surmeier et al., 2010), and recent experimental work implicates mitochondrial Ca2+ dysregulation (Celsi et al., 2009). In particular, the Cav1.3 calcium channel on striatopallidal neurons expressing the D2

dopamine receptor has been linked to the degeneration of dendritic spines on striatal projection neurons. Particular to this chapter, the density of spines within the striata nigra have been found to be greatly reduced for Parkinson's patients, along with a reduction in their dendritic arbors (Gerfen, 2006).

Earlier theoretical models have studied how activity-dependent calcium release from mitochondria may alter dendritic spine morphology (Verzi et al., 2004; Verzi & Baer, 2005), and how activity may directly affect the density and distribution of spines along the dendrite (Verzi et al., 2004). Models have demonstrated that in dendrites with excitable spines, generation and propagation of action potentials depend on the morphology and spatial distribution of spines (Verzi et al., 2004; Verzi & Baer, 2005). A wave can propagate if localized excitatory synaptic input into spine heads causes a few excitable spines to fire, initiating a chain reaction of spine firings along the dendrite. Baer and Rinzel (1991) found that a sustained wavelike response is possible for a certain range of spine densities and electrical parameters. They found that propagation is precluded when spine stem resistance is either too small or too large and that success or failure of local excitation to spread as a chain reaction depends on the spatial distribution of spines (Baer and Rinzel, 1991).

It is painfully obvious that Parkinson's is a complex disorder, involving alterations in brain chemistry, morphology and activity, and an enhanced understanding of the interdependence of these processes will increase our understanding of this devastating disease. This chapter will offer several models to consider these relationships within the striata nigra.

2. Methods

This section develops variations on models for activity-dependent and calcium-regulated spine density and morphology, with age-, temperature- and disease-related changes in the dendritic arbor of the Parkinsonian striata nigra. Dopamine has been implicated as a thermoregulator for dopaminergic neurons (Brown et al., 1982), along with the observation of localized variations in neuronal temperature (Guatteo et al, 2005). Since ionic activity is the driving force in the following models, a study of how temperature may affect the magnitude and frequency of activity is an implicit model for dopamine-dependent levels of neuronal activity.
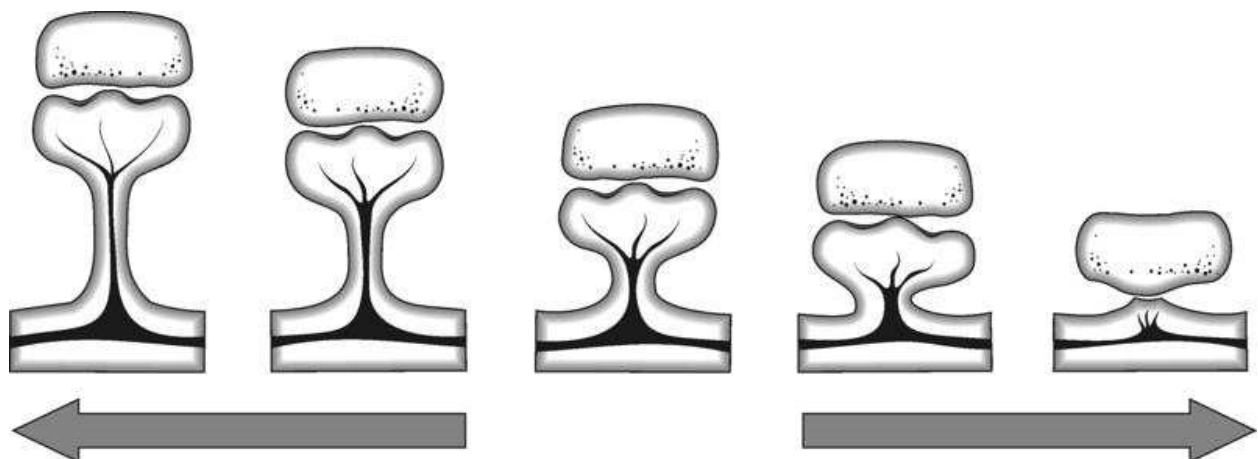

Fig. 1. **Spine loss as a contributor in neuronal death.** Spines may be reabsorbed into the dendrite, or stretch to a point where resistance from the spine stem hinders signal transduction, contributing to neuronal isolation.

2.1 Activity-dependent spine densities

Spines are mushroom shaped protrusions from the soma or dendritic arbor of a neuron, and the loci of 90% of excitatory synaptic connections. Spine loss is observed in normal aging, with an accelerated loss for patients with Parkinson's disease. A dendrite may be populated with thousands of spines of different sizes, shapes and configurations. The basic model for a dynamic distribution of spines is based on Baer and Rinzel's cable theory (1991), where the membrane potentials vary continuously in space and time. Spines interact indirectly by voltage spread along the dendritic cable.

Consider a dendrite with passive membrane properties of a prescribed (dimensionless) electrotonic length (*el*), studded with a population of spines. The spine density $\bar{n}(X,t)$ represents the average number of spines per unit *el*. At each location X, the spines deliver current $\bar{n}I_{ss}$, where I_{ss} represents the current flowing through an individual spine stem. The spine stem is modeled as a lumped Ohmic resistor, (Segev & Rall, 1988), so that the stem current is expressed as a voltage drop across the resistor, $R_{ss}(M\Omega)$:

$$I_{ss}(X,t) = \frac{V_{sh}(X,t) - V_d(X,t)}{R_{ss}} \ . \tag{1}$$

The variables V_{sh} *(mV)* and V_d *(mV)* are, respectively, the membrane potential in the head and dendritic base. If potential in the spine head is larger than in the dendrite, I_{ss} >0.0, then the current is flowing from spine head to base. Conversely, if the potential in the base is larger than in the spine head, I_{ss} <0.0, then current flow is from base to head. The spine stem resistance (R_{ss}) represents the ratio of specific cytoplasmic resistance to cross-sectional area, integrated over the length of the stem. A constriction at any location along the stem would decrease the cross sectional area, significantly increasing R_{ss}. Likewise, a stem occlusion could significantly increase internal cytoplasmic resistance, and increase R_{ss}.

The electrical potential in a passive dendrite, studded with $\bar{n}$ spines per unit length, satisfies the cable equation

$$\tau_m \frac{\partial V_d}{\partial t}(X,t) = \frac{\partial^2 V_d}{\partial X^2} - V_d + R_\infty \bar{n} I_{ss} \ , \tag{2}$$

where τ_m is the membrane time constant, R_∞ is the cable input resistance, and $\bar{n}$ is the average density of spines at each location $X = x/\lambda$, with $\lambda(\mu m)$ the physical length. The model assumes that the dendrite has sealed-end boundary conditions and that both the dendrite and spines have zero resting potentials.

An equation for the membrane potential in each spine head is obtained from a current-balance relation for the capacitive, ionic, synaptic and spine stem currents:

$$C_{sh} \frac{\partial V_{sh}}{\partial t}(X,t) = -I_{syn} - I_{ion} - I_{ss} \ . \tag{3}$$

The term I_{ion} represents ionic currents passing through the spine head membrane and I_{syn} the synaptically applied current. In a simulation involving spines with passive membrane properties, the ionic current is modeled simply as the ratio of head potential to resistance:

$$I_{ion}(X,t) = \frac{V_{sh}(X,t)}{R_{sh}}. \tag{4}$$

If the spines are considered to have excitable membrane properties, Hodgkin-Huxley kinetics model temperature- and voltage-dependent ion channel currents (Hodgkin & Huxley, 1952), and

$$I_{ion}(X,t) = \gamma A_{sh} \left[g_{NA} m^3 h(V_{sh} - V_{NA}) + g_K n^4 (V_{sh} - V_K) + g_L(V_{sh} - V_L) \right]. \tag{5}$$

The parameters γ and A_{sh} represent channel density and spine head area, and the gate activation/inactivation variables m, n and h satisfy first-order rate equations with voltage-dependent time constants and steady-state functions (Hodgkin & Huxley, 1952). The parameters V_{Na}, V_K and V_L are synaptic reversal potentials for sodium, potassium and leakage currents, with maximal conductances of g_{Na}, g_K and g_L, respectively.

Synapses over a small interval are activated by applying a brief synaptic conductance to the spines in that interval

$$I_{syn} = g_p \frac{t}{t_p} \exp\left(1 - \frac{t}{t_p}\right)(V_{sh} - V_{syn}), \tag{6}$$

where V_{syn} is the synaptic reversal potential. The synaptic current is applied periodically, maximizing to g_p, when $t = t_p$ in each period.

Let I_{ss}, the spine stem current from Eq. (1), be a measure for local activity. Then, the density of spines at any location X along the dendrite is assumed to be a dynamic variable that changes slowly over time and depends on electrical interactions between the spine head and dendritic shaft, as measured by the spine stem current. Let $\bar{n}(X,t)$ the average density of spines per unit el be a dynamic variable that changes slowly over time and space, and depends on electrical interactions between the spine head and the dendritic base. In general, the change in $\bar{n}$ is assumed to be bounded and proportional to I_{ss}. Then,

$$\frac{\partial \bar{n}}{\partial t}(X,t) = \varepsilon_n \mathrm{K}_n I_{ss} \left(1 - \frac{\bar{n}}{n_{max}}\right)(\bar{n} - n_{min}), \tag{7}$$

describes this change, where $\varepsilon_n \ll 1$ is dimensionless, and K_n is a positive parameter scaled to cable input resistance. Density increases in response to local synaptic activity, decreases in response to centripedal flow, and remains unchanged in regions experiencing no measurable level of activity. Changes in spine density depend on changes in I_{ss}, which in turn depend on the integrative properties of the surrounding membrane and synaptic activity. A more detailed derivation of this model may be found in Verzi et al. (2004).

2.2 A model of dendritic spine loss with age and Parkinsonism
An early model for idiopathic Parkinsonism considered the temporal profile for neurodegeneration in dopaminergic neurons, assuming a linear loss for normal aging, and a quadratic or exponential loss consistent with the duration of symptoms (Schulzer et al., 1994). Since ten percent of these neurons seem to survive, a lower bound was placed on the

temporal function. A reduction in dendritic spines may be considered as a reduction in axo-dendritic synapses, and a total loss of synaptic contact may be considered as neuronal isolation or cell death.

To consider the implications of activity-dependent spine densities in the substantia nigra, consistent with age-related linear and Parkinson-related quadratic loss of dopaminergic neurons, one could remove the upper bound for spine density, and append linear and quadratic terms to Eq. (7), replacing it with

$$\frac{\partial \bar{n}}{\partial t}(X,t) = \varepsilon_n K_n I_{ss}(\bar{n} - n_{\min}) - \delta(\bar{n} - n_{\min}) - \theta(\bar{n} - n_{\min})^2. \tag{8}$$

2.3 A model for the interdependence of activity, calcium and dendritic spine morphology

While activity affects, and is affected by the distribution and density of spines along the dendrite, so also are the structures of individual spines. Earlier theoretical models (Verzi et al., 2004; Verzi & Baer, 2005) have considered how activity-dependent calcium-regulated dendritic morphology could alter neuronal firing patterns to enhance or impede the efficacy of a neuronal network. This was based on experimental observations that a moderate amount of neuronal activity may release Ca2+ from mitochondria, reshaping dendritic spines to increase synaptic efficacy, but that too much activity may raise Ca2+ within the cytosol to a caustic level and cause the spines to pull away from the synaptic connection, thereby contributing to isolation of the neuron (Harris, 1999).

This section considers how activity-dependent free intraspine calcium may function as a second messenger in regulating continuous changes in dendritic spine morphology. For a fixed distribution of spines along the dendrite, let the spine stem resistance R_{ss} (reciprocal of conductance) be a measure for dynamic spine stem morphology. Spines with longer and thinner stems, or those deformed by organelle occlusions, such as mitochondria or endoplasmic reticula, generally have higher measures of stem resistance and are more isolated from the dendrite, while those with shorter and wider stems generally have lower input resistance, and may be more electrically connected to the dendrite. A continuum model consistent with the above assumptions utilizes Eqs. (1-6), replacing Eq. (7) in the model for activity-dependent dendritic spine densities with the following slow subsystem for calcium-regulated dendritic spine morphology:

$$\frac{\partial C_a}{\partial t}(X,t) = -\varepsilon_C (C_a - C_{\min}) + |I_{ss}| / K_C \tag{9}$$

$$\frac{\partial R_{ss}}{\partial t}(X,t) = -\varepsilon_R \left(\frac{C_a}{C_{crit}} - 1\right)\left(\frac{C_a}{C_{\min}} - 1\right)\left(1 - \frac{R_{ss}}{R_{\max}}\right)(R_{ss} - R_{\min}) \tag{10}$$

In this model, local activity is measured by the magnitude, or absolute value, of the spine stem current, regardless of direction. Local calcium levels increase, so long as $|I_{ss}|$ is large enough, with respect to the current saturation of calcium, relative to a minimum amount. The parameter K_C scales this relationship. The model prescribes a critical intraspine calcium level (C_{crit}), consistent with Harris (1999), as threshold for whether or not local spines become long and thin or short and stubby. The stem resistance increases for $C_a < C_{crit}$

(subcritical), modeling spine stem elongation, and decreases for $C_a > C_{crit}$ (supercritical), modeling spine stem shortening.

Now the spine density ($\bar{n}$) is no longer dynamic, but the spine stem resistance ($R_{ss}(X,t)$) is a bounded, dynamic function of activity and free intraspine calcium, relative to some minimal level. When synaptic activity is present, stem resistance approaches steady-state if R_{ss} approaches the bounds of R_{max} or R_{min}, or if I_{ss} drives C_a to C_{crit}.

For ε_C and $\varepsilon_R << 1$, the slow subsystem described in Eqs. (9-10) connects to the fast equations for activity (Eq. 1-6) by I_{ss} in Eqs. 2, 3 and 9, and by R_{ss} in Eqs. 1 and 10. In the absence of activity, the system approaches equilibrium, since C_a approaches C_{min} when $I_{ss} = 0$, and $\partial R_{ss} / \partial t = 0$ when $C_a = C_{min}$. In the model, the cable input resistance (R_∞) is fixed, while R_{ss} varies over time and space. The difference between spine head and base potentials in Eq. (1) becomes negligible since $V_{sh} \to V_d$ in Eq. (1) as $R_{ss} \to R_{min}$, imposing a kinetic upper bound on calcium (i.e. $|I_{ss}| = |V_{sh} - V_d| / R_{ss}$ becomes small enough that Eq. (9) is negative).

2.4 A discussion of temperature-dependent neuronal firing patterns

Hodgkin & Huxley (1952) hypothesized in their famous study of the squid giant axon that sodium movement depends on the distribution of charged particles that allow sodium to pass through the membrane, so that changes in membrane permeability are a function of membrane potential, rather than current. They supposed that the rate of movement of the activating particles determined the rate at which the sodium conductance approached its maximum, concluding that temperature had a large effect on this rate, and the frequency for repetitive firing and recovery. While of opposite charge, similar statements were made about changes in sodium permeability.

Many theoretical models utilize Hodgkin-Huxley kinetics for excitable (or active) membrane response, with an implicit adjustment for temperature. The gating variables *m*, *n* and *h* in Eq. (5) consider the voltage-dependent probability that the sodium and potassium channels are open as

$$\frac{dm}{dt} = \alpha_m(V_{sh})(1-m) - \beta_m m$$
$$\frac{dh}{dt} = \alpha_h(V_{sh})(1-h) - \beta_h h \qquad (11)$$
$$\frac{dn}{dt} = \alpha_n(V_{sh})(1-n) - \beta_n n$$

where the voltage-dependent, gating functions $\alpha_i(V_{sh})$ and $\beta_i(V_{sh})$ *for i=m, n* and *h*

$$\alpha_m(T,V_{sh}) = \Phi(T)\frac{0.1(25-V_{sh})}{\exp(0.1(25-V_{sh})-1)}$$
$$\beta_m(T,V_{sh}) = \Phi(T)\exp(-V_{sh}/18)$$
$$\alpha_h(T,V_{sh}) = \Phi(T)0.07\exp(-V_{sh}/20)$$
$$\beta_h(T,V_{sh}) = \Phi(T)\frac{1}{\exp(0.1(30-V_{sh})+1)} \qquad (12)$$
$$\alpha_n(T,V_{sh}) = \Phi(T)\frac{0.01(10-V_{sh})}{\exp(0.1(10-V_{sh})-1)}$$
$$\beta_n(T,V_{sh}) = \Phi(T)0.125\exp(-V_{sh}/80)$$

are adjusted for variation from Hodgkin & Huxley (1952) results obtained at $T = 6.3$ Celsius (C), by the factor:

$$\Phi(T) = 3^{\left(\frac{T-6.3}{10}\right)}. \tag{13}$$

Modeling an increase in temperature in Eq. (13) decreases the time-duration for an action potential, with a decrease in maximal amplitude (see Fig. 2 below). Conversely, a decrease in temperature stretches out the action potential over time and increases the maximum membrane potential. Increasing temperature also raises the voltage threshold for action potential generation, and decreasing temperature lowers this threshold (Fitzhugh, 1966).
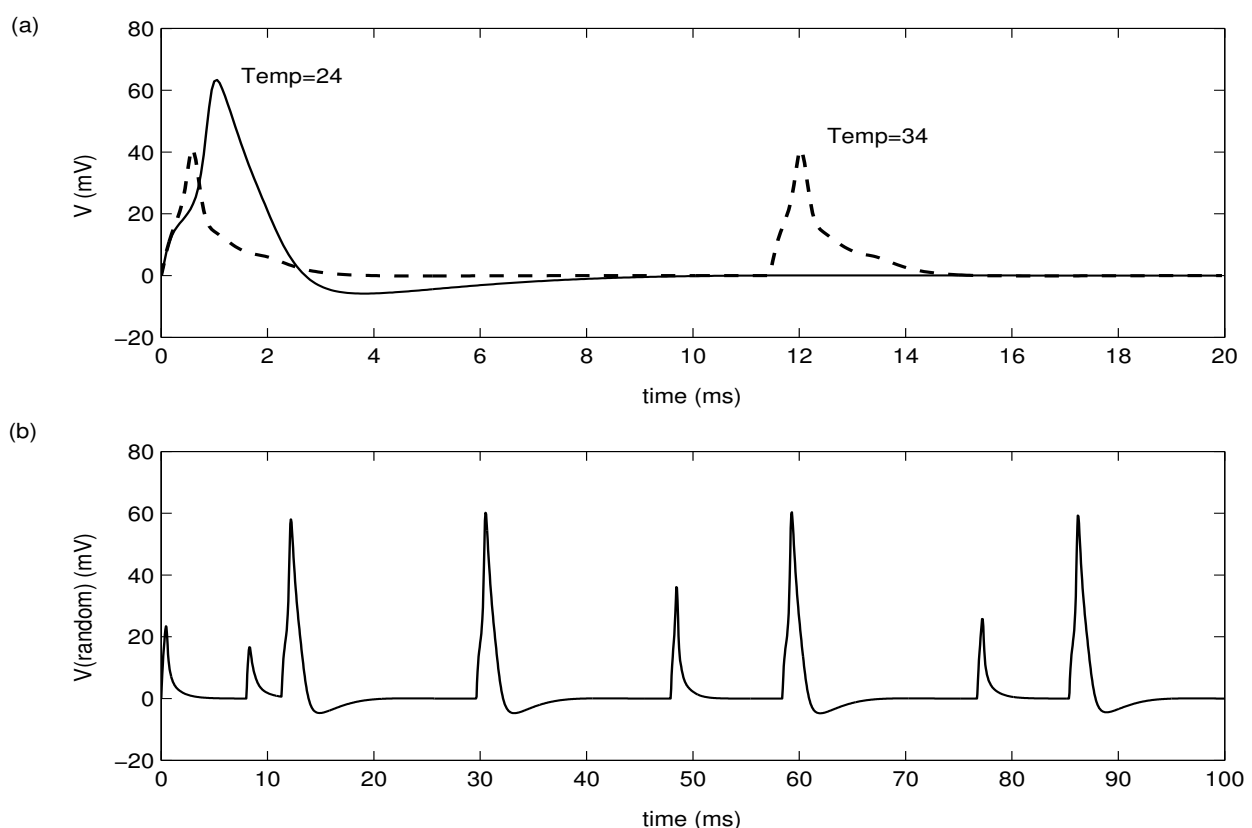

Fig. 2. **Temperature-dependent variations in neuronal activity.** The magnitude and shape of neuronal response depends on localized membrane temperature. Periodic synaptic activation is temperature-dependent.

Earlier theoretical studies demonstrated the interdependence of dendritic activity, morphology and chemistry for fixed temperature and activation periods (Verzi et al., 2004; Verzi & Baer, 2005). This chapter considers how slow changes in morphology and chemistry affect and are affected by temperature-dependent changes in ionic activity. In most of the simulations, temperature is defined iteratively for each activation cycle, remaining constant for the duration of a cycle k as

$$T(1) = \omega, \text{ and } T(k+1) = T(k) + \sigma. \tag{14}$$

For $|\sigma| \ll 1$, continuous changes in temperature describe a simulation for warming if $\sigma > 0$ and cooling for $\sigma < 0$. Since studies have observed a decrease in temperature and firing frequency in Parkinsonism (Guatteo et al., 2005), simulations will, likewise, consider the effect of temperature-dependent continuous changes in activation frequency, describing the period between synaptic firings from Eq. (6) as

$$P = \upsilon - \rho T . \tag{15}$$

For $\rho > 0$, the length of an activation cycle is inversely proportional to temperature for an increasing period during gradual cooling, and decreasing period for warming. Figure 2a displays two temperature-dependent magnitudes for excitable membrane response (Eq. 5). Note the slower rise in sodium to a greater maximum for cooler temperatures (Fitzhugh, 1966). In Fig. 2b, temperature is random on T in [24,39] to display the range of magnitudes and frequencies from Eq. (15).

3. Results

In the simulations that follow, the models are numerically integrated using a semi-implicit Crank-Nicholson/Adams-Bashforth finite differencing method. The spatial step is set to $\Delta X = 0.4$, with a corresponding time step of $\Delta t = .005$ for simulations with R_{ss} of higher values, and $\Delta X = 0.1$, with $\Delta t = .0005$ to maintain stability for R_{ss} of lower values. Computations are performed in Fortran double-precision on a *Sun-Solaris 9* computer. Since, in reality, a significant increase in spine density takes place on a time scale of hours to days and individual action-potentials are on a time scale of milliseconds, the computation time for a simulation could be on the order of hours. For most simulations, the synaptic input is repeated at greater than or equal to 8 *ms*, long enough to allow potentials in the head and dendrite to return to resting values. For each of the time scaling values that define slowly changing variables, one must identify a value that preserves the basic dynamics of the system as $\varepsilon_i \to 0$. Using a computer animation program with uniform activation periods, an initial value is chosen to animate the time course at three spatial locations over 60 synaptic events for a typical run involving the development of a propagating wave. Then each ε_i is halved, and simulations are repeated for 120 activation cycles. The results are superimposed, using every-other cycle of the 120-cycle simulation. The process is repeated several times, successively halving ε_i and doubling superimposed cycles, until the animations converge at ε_i^*. Then ε_i is set to ε_i^* for each *i*, sufficiently small and computationally efficient, without compromising the integrity of the dynamics for smaller values that define chemical and morphological changes over hours to days.

3.1 Dendritic spine loss with age and Parkinsonism

Equations (1-3) and (8) are used in four separate simulations, with initially 23 spines/unit *el*, uniformly distributed over a dendrite of length 3. Spines over X in [0, 0.2] are activated every 10 *ms* with Eq. (6). In two of the simulations, the spines are considered to have passive membrane properties, merely passing the signal along the dendrite, so that the ionic membrane current is modeled with Eq. (4). In the other two simulations, the spines are considered to have excitable, or active membrane properties to modulate a signal on its way

Cable and Spine Model	τ_m	Membrane time constant	$2.5ms$
	R_∞	Cable input resistance	$1233M\Omega$
	λ	Physical length	$180\mu m$
	C_{sh}	Spine head capacitance	$C_m A_{sh}$
	C_m	Membrane capacitance	$1mF/cm^2$
	A_{sh}	Spine head surface area	$1.31/\mu m^2$
	R_{sh}	Spine head membrane resistance	$10.02 \cdot 10^{11}\Omega$
	R_{ss}	Spine stem resistance	See simulations
Spine Density Models	ε_n	Density time constant	$8.02 \cdot 10^{-6}$
	K_n	Scaling parameter	10^9
	n_{max}	Upper bound	$50/e.l.$
	n_{min}	Lower bound	$0/e.l.$
	δ	Linear rate of loss	10^{-3}
	θ	Quadratic rate of loss	10^{-4} or 0
Calcium-Morphology	ε_C	Calcium time constant	$3 \cdot 10^{-3}$
	ε_R	Resistance time constant	$7.5 \cdot 10^{-5}$
	K_C	Scaling parameter	$3.3 \cdot 10^{-10}$
	C_{min}	Calcium lower bound	$5nM$
	C_{crit}	Calcium critical level	$300nM$
	R_{min}	Stem resistance lower bound	$90M\Omega$
	R_{max}	Stem resistance upper bound	$2000M\Omega$
Kinetics	γ	Channel density scale factor	2.5
	g_{NA}	Maximal sodium conductance	$120mS/cm^2$
	g_K	Maximal potassium conductance	$36mS/cm^2$
	g_L	Maximal leakage conductance	$0.3mS/cm^2$
	V_{NA}	Sodium reversal potential	$115mV$
	V_K	Potassium reversal potential	$-12mV$
	V_L	Leakage reversal potential	$10.5989mV$
Synaptic activation	g_ν	Peak synaptic conductance	$0.074nS$
	t_p	Time to peak synaptic conductance	$0.2ms$
	V_{syn}	Synaptic reversal potential	$100mV$
Temperature and Period	ω	Initial temperature	See simulations
	σ	Rate of change in temperature	See simulations
	υ	Period scaling constant	40
	ρ	Rate of change in period	0.8

Table 1. Table of model parameters

to the soma, modeled here with kinetics from Eq. (5). Figure 3 graphs results for two passive simulations (left) and two active simulations (right), reporting results for spines "downstream" of the synaptic activation at *X=0.5*, to observe local response without input current from the axon.

In Eq. (8), spine density may increase for sufficiently high levels of activity to offset linear and/or quadratic loss due to age or the onset of Parkinson's disease, respectively. The spine density over time is graphed in Fig. 3a for two passive (left) and two active (right) simulations, superimposing results for linear assumptions for aging only (*NL*) over linear and quadratic assumptions for both aging and Parkinsonism (*NQ*).

Simulations with passive or active membrane in dendritic spines shows a linear decrease when $\theta = 0$, to model only age-related loss of spines in Eq. (8), and a quadratic decrease in spine density when θ is positive, modeling the effect of both aging and Parkinson's disease on the loss of synaptic connections. Parameter values chosen here are set to emphasize qualitative differences for age- and Parkinson-related spine loss, and results are observed over a relatively short period of time. Since the action potential is rapidly shut down by spine loss, the rate of spine loss is similar from passive to active simulation.
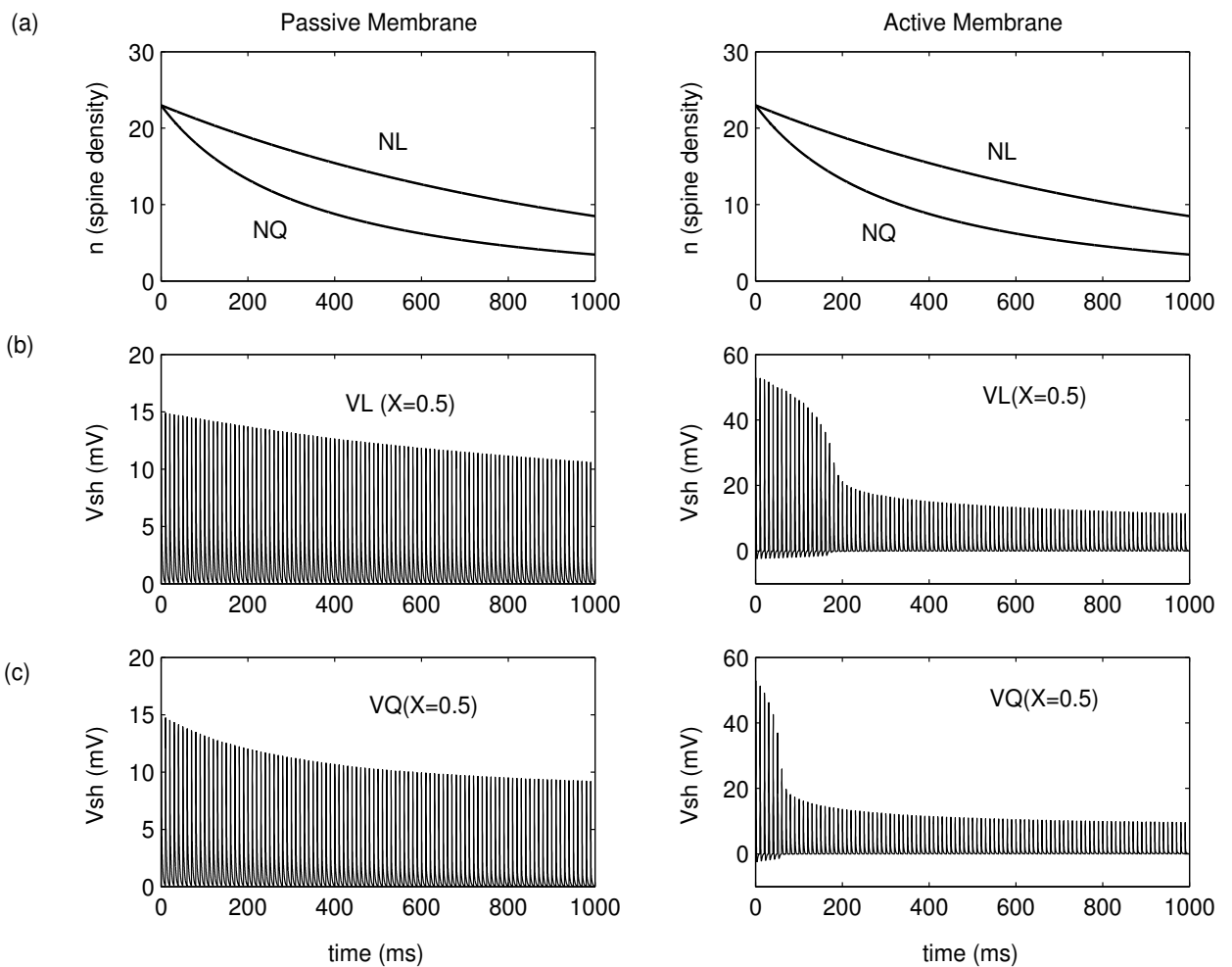

Fig. 3**. Age- and Parkinson- related dendritic spine loss**. Spine density is modeled to decrease linearly with age, and quadratically after the onset of Parkinson's disease.

Figure 3b graphs the time course for spine head potential in the linear simulation (*VL*). In the passive simulation (left) peak potential in each 10-*ms* activation cycle decreases linearly with *NL* (above). Spine density is initially large enough to cause an action potential in the active spine simulation (right), but quickly decreases below threshold *NL*=20, so that maximum potentials decrease linearly for the duration of the simulation. In Fig. 3c, potential in the spine heads is graphed over time for the quadratic simulation (*VQ*). Peak potentials decrease quadratically with *NQ* in Fig. 3a for the passive simulation (left). In the active simulation (right), *VQ* loses its nonlinear response much earlier, when *NQ* falls below threshold to generate an action potential for spines with stem resistance uniformly set to $R_{ss} = 1240 M\Omega$. Spine density decreases at each time step linearly or quadratically, with a decrease in the rate of change as $\bar{n} \to n_{\min} = 0$. The strength of the signal passed to the dendrite decreases proportional to the density of spines.

3.2 Temperature-regulated dendritic spine density

To model how cooling temperatures due to dopamine depletion affect the density of spines and resultant efficacy of signal transduction in the dendrite, Equations (1-3) and Eq. (7) are used in a single simulation for spines with excitable membrane properties. The initial spine density is set to 23 spines/unit *el*, uniformly distributed over a dendrite of length 3. Since the spines are assumed active, I_{ion} from Eq. (5) models voltage-dependent membrane kinetics. Spines are stimulated over *X* in [0, 0.2] with I_{syn} from Eq. (6) that peaks at $t_p = 0.2ms$ in each activation cycle. Different in this simulation, the period between activations is temperature-dependent from Eq. (15) with υ and ρ chosen to vary the period from 8 to 20 *ms* over a temperature range of 39 to 24° *C*. The temperature decreases from $\omega = 39$ in Eq. (14) at a rate of $\alpha = -0.05$.

In Fig. 4a (left) temperature changes with each cycle, with the rate of change decreasing as cycles grow longer for cooler temperatures. On the right side of Fig. 4a, spine density is graphed in a spatial profile over the entire dendrite at three frozen moments in time: The initial condition is indicated by the top dashed line at $\bar{n} = 23$, with a slight rise in density over the activation site at *t*=1000 *ms*, with a decrease in densities downstream. After 5000 *ms*, density has significantly decreased over the entire length of the dendrite.

In Fig. 4b, spine head potential is graphed over time within the activation site (left) and downstream (right). Downstream, $I_{ss} \le 0$ until the spines initiate their own action potential to propagate the signal. At *t*=1000 *ms*, action potential generation begins at *X*=1.0, but spine densities continue to decrease across the dendrite (4a right) , even in the presence of a propagating wave, due to the increasingly longer periods with little or no activity. Shorter cycles for higher temperatures may be observed in the dark shading (*t*<800*ms*), compared to the shading for longer periods (*t*>3000).

Spine density is an important parameter for action potential generation and propagation, since more spines increase membrane potential per location *X*. While the initial density of 23 would be sufficient for an action potential under normal temperatures, the higher voltgage-threshold for *T*=39 degrees prevents generation at the beginning of the simulation. The voltage-dependent gating functions α_i and β_i from Eq. (12) contain a temperature-dependent factor from Eq. (13) that increases the magnitude and decreases the voltage-threshold for action potential response under cooler temperatures (Fitzhugh, 1966). Figure

4c graphs the change in density over time within the activation site (left) and downstream (right). Note the rate of decrease is constant in the activation site (left), but greater downstream (right) in the absence of local action potential generation.
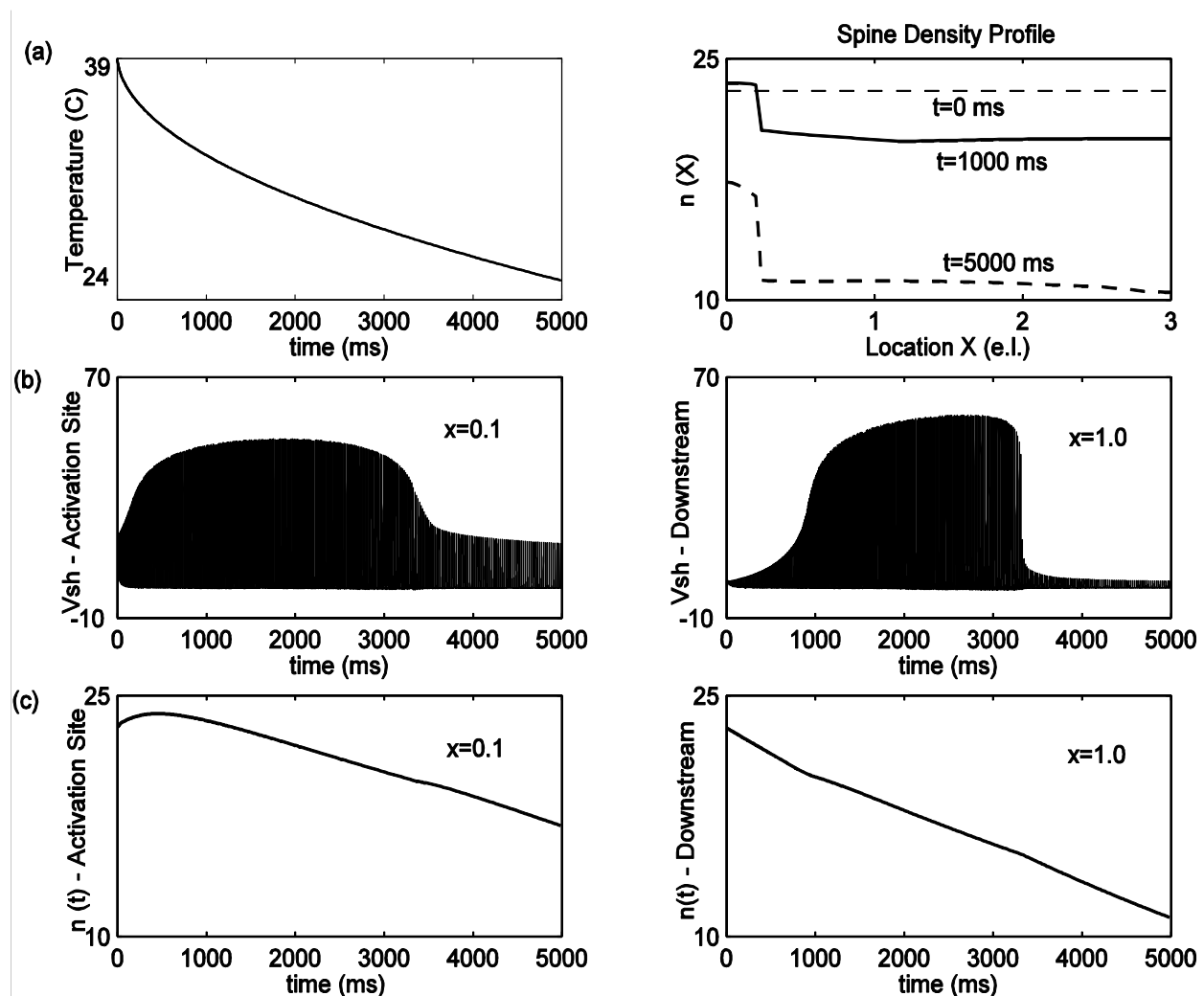

Fig. 4. **Temperature regulated excitable dendritic spine densities.** Spine densities decrease for cooler temperatures and longer activation cycles, even in the presence of action potential generation and propagation.

3.3 Steady-state calcium regulated spine morphology

The model for calcium-regulated spine morphology demonstrates how variations in the frequency of synaptic activation may affect the shape and efficacy of dendritic spines (Verzi et al., 2004; Verzi & Baer, 2005). Eqs. (1-3) and (9-10) model the interdependence of activity, chemistry and morphology for a fixed population of spines along the dendrite. Using the stem resistance as a measure for morphology, the model identifies a variation in steady-states for calcium and spine shape, based on the frequency of activation.

Figure 5 illustrates two such steady-states. A uniform density of 23 spines/unit *el* are distributed along a dendrite of length 3. They are assumed passive, so that Eq. (4) describes the ionic current. Now the spine density is fixed, but the morphology of each spine is a

dynamic variable, measured by the spine stem resistance, $R_{ss}(X,t)$. The morphology depends on the local level of calcium $C_a(X,t)$ (Eq. 10), which, in turn, is regulated by the magnitude of local activity, as measured by $|I_{ss}|$ (Eq. 9). Initially, stem resistance and calcium are uniformly set to $R_{ss} = 750M\Omega$, and $C_a = 15nM$. Spines are activated over X in [0, 0.2] with Eq. (6) every 20 ms or 50 Hz (left), and every 8 ms or 125 Hz (right), and results are shown for spines under synaptic activation. The parameter $C_{crit} = 300nM$ for Eq. (10), so that R_{ss} increases when C_a is below the dashed line in Fig. 5a, and decreases when C_a is above the dashed line.

(a)

(b)
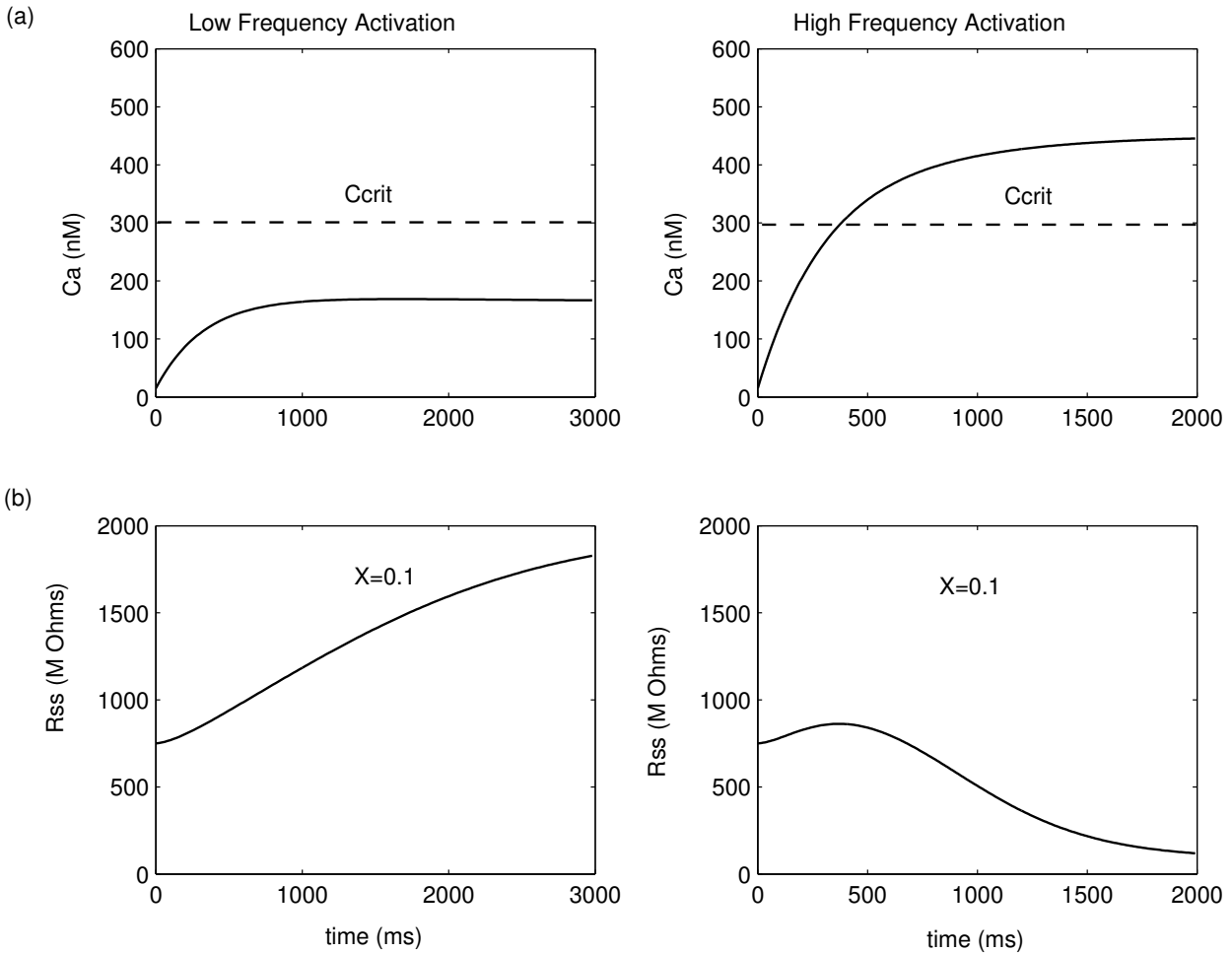
Fig. 5. **Calcium-regulated dendritic spine morphology.** Steady-state solutions depend on the frequency of synaptic activation. If calcium is supercritical/subcritical, the spines display higher/lower input resistance.

The upper bound for free intraspine calcium settles to a sub-critical steady-state for low-frequency activation (Fig. 5a left) and a super-critical steady-state for high-frequency activation (Fig. 5a right). In Fig. 5b (left), stem resistance rises rapidly as calcium increases, but reaches an inflection point to slow its ascent toward R_{max} as calcium approaches steady-state, for low-frequency synaptic activation. In Fig. 5b (right), stem resistance increases while calcium is below C_{crit}, and begins to decrease toward R_{min} when calcium becomes super-critical for high-frequency stimulation.

3.4 Frequency-dependent calcium regulation for spines with passive membrane properties

It has been observed in Parkinson's disease that a decrease in temperature causes a reduction in the frequency of neuronal firing in the striata nigra, along with a decrease in the amount of free interstitial calcium. Likewise, an increase in temperature has been shown to cause an increase in the frequency of firing, with an increase in free calcium, citing temperatures ranging from -10 to +5 degrees from 34 C (Guatteo et al., 2005). While temperature is not explicit in the model for spines with passive membrane properties, it may be inferred from the positive correlation between temperature and firing frequency.

Figure 6 illustrates two simulations to study the effect of a continuous change in temperature-dependent frequency variations from Eq. (15) for the calcium-regulated spine morphology model, using Eqs. (1-3) to model rapid changes in activity and Eqs. (9-10) for the slow subsystem of calcium and spine stem resistance, as in the steady-state simulations from Fig. 5 above. Once again, a dendrite of length 3 is assumed to have a fixed density of 23 uniformly distributed passive spines/unit el, with initial uniform morphology $R_{ss} = 750M\Omega$. This time, initial free calcium is uniformly set to $C_a = 150nM$. Since the spines are assumed to have passive membrane properties, the ionic current is modeled with Eq. (4).
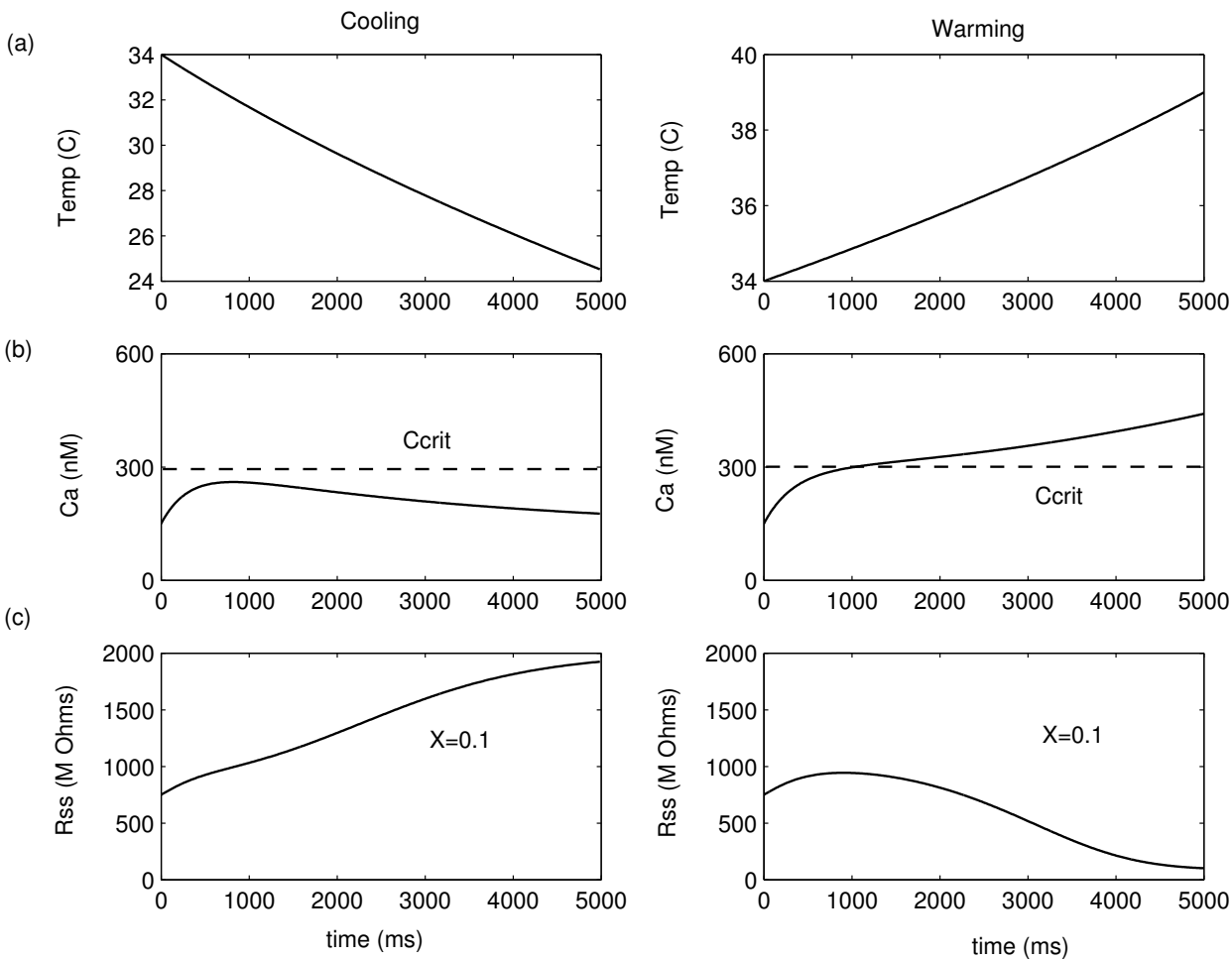

Fig. 6. **Frequency-dependent calcium regulation of passive dendritic spine shape.** Longer/shorter periods between activations cause calcium to decrease/increase and spine length to increase/decrease.

The period between activations is modeled to be temperature-dependent from Eq. (15), with υ and ρ chosen to, again, vary the period from 8 to 20 *ms* over a temperature range of 39 to 24 degrees. Figure 6a graphs temperature over 5000 *ms* for cooling (left) and warming (right). The initial temperature is set to change from $\omega = 34$ in Eq. (14) at a rate of $\alpha = -0.03$ in each activation period for the simulation over 10 degrees of cooling in Fig. 6 (left), and $\alpha = 0.01$ for the simulation over 5 degrees of warming in Fig. 6 (right), since activation cycles are much shorter over time for warmer temperatures.

In Fig. 6b, calcium does not approach equilibrium, but remains subcritical during cooling (left), and climbs steadily beyond C_{crit} as both the temperature and frequency of activation increase during warming (right). In response, Fig. 6c displays an increase in stem resistance toward maximum as the temperature cools (longer activation period) and decreases toward its minimum under warming conditions (shorter activation period), consistent with experimental observations (Guatteo et al., 2005). It is interesting to note that the balance between local activity and free intraspine calcium from Eq. (9) changes sign so that calcium begins to decrease (6b left) when the length of each activation period equals 13.6 *ms* (*T=32 C)*. It is also interesting to observe that calcium increases almost linearly with warming (6b right) after stem resistance begins to decrease.

3.5 Temperature-dependent calcium regulation for spines with active membrane properties

Different from the previous simulation for calcium regulated passive spine morphology, a simulation of the same model for spines with active membrane properties has a direct link to temperature. Recall that the gating functions in the Hodgkin-Huxley kinetics are adjusted for temperature by Eq. (13). Once again, Eqs. (1-3) and (9-10) model activity-dependent calcium, and calcium-regulated spine morphology, under the assumption that the period between synaptic activations is a function of temperature from Eq. (15). Twenty-five spines/unit *el* with excitable membrane properties are uniformly distributed across a dendrite of length 3. Spines over X in [0, 0.2] are activated with I_{syn} from Eq. (6), and the active ionic membrane currents are modeled by Eq. (5).

Figure 7 illustrates results from a simulation for temperatures cooling (Eq. 14) from $\omega = 34$ to 24 degrees at a rate of $\sigma = -0.03$ degrees/activation cycle. Initial values for calcium and spine stem resistance are uniformly 15 *nM* and 900 *MΩ*, respectively. While the rate of cooling is constant between cycles, Fig. 7a (left) again shows a reduction in the rate of cooling over time, since the length of activation cycles lengthens as the temperature cools. In Fig. 7a (right) calcium rises quickly to supercritical, since voltage is above threshold to generate an action potential for the current values of stem resistance and temperature. Voltage in the spine heads under synaptic activation rises in the presence of an action potential briefly in Fig. 7b (left) until the temperature drops below. It is interesting that the magnitude of an action potential may be higher for cooler temperatures, but the voltage threshold for generation decreases as temperatures cool (Fitzhugh, 1966).

Stem resistance rises when calcium is below the dashed line for C_{crit} and falls when calcium is above it in Fig. 7 (right). When action potential generation ceases, $|I_{ss}| / K_c < \varepsilon_c (C_a - C_{min})$ in Eq. (9), so that the change in calcium is negative and calcium falls below subcritical to a steady-state balance between these two terms. However, since the steady-state is subcritical, as in Fig. 5 for low frequency activation, R_{ss} continues to rise for the duration of the simulation. After

6500 *ms*, stem resistance has returned to its initial value of 900 *MΩ* (7b right), but the maximum spine head potential has fallen from 28 *mV* to 13 *mV* for the same number of spines with the same morphology. The temperature has fallen from 34 to 24, affecting voltage threshold to generate an action potential. Note also the hyperpolarization of head potential in the presence an action potential at the beginning of the simulation, and after 2500 *ms*, when the temperature has fallen below 30. Compare this result with Figs. 3 and 4 for dynamic spine density where there is no hyperpolarization for passive membrane simulations, and only in the presence of an action potential for active simulations.
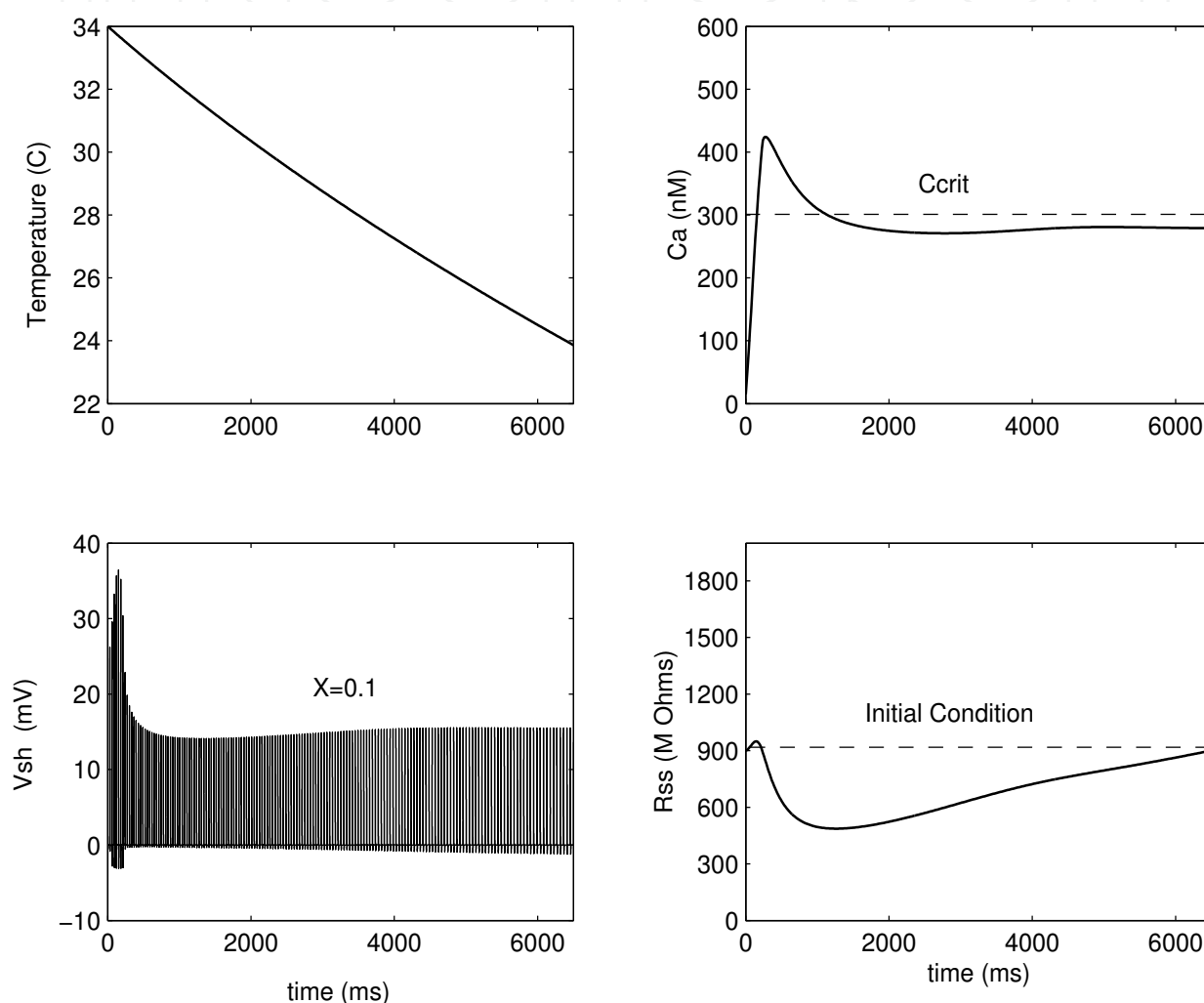
Fig. 7. **Temperature-dependent calcium regulation of active dendritic spine morphology.** Cooler temperatures lengthen the period between synaptic activations, decreasing the amount of local activity and free intraspine calcium levels, which increases spine stem length and input resistance.

4. Conclusions

It is challenging to consider the long-term effect over months to years of activity that scales on the order of milliseconds. The length of time for density and structural transition in the

models presented depends on the magnitude of ε_i, for $i=n, C, R$, selected here for computational efficiency. To achieve the results shown in this paper over several months, one would need to set the rate of change in spine structure on the order of 10^{-25}. An alternative to speed up computation time in systems with periodic activation would be to exploit the fact that the slow variables are piecewise continuous over time and relatively constant within each activation cycle. One might then use the average measure of local activity (such as I_{ss}) in each cycle to compute changes in the slow system at the end of each cycle of length P, rather than integrating the entire system at each time step. While simulations in this paper consider repetitive input to a fixed site along the dendrite, an interesting question for future work is to observe long term effects for simulations where the activation site is randomly selected in each cycle.

The results in this chapter agree with earlier generalized neuronal studies for spine density (Annis et al., 1994) and morphology (Harris, 1999), and specifically to recent studies within the striata nigra for Parkinsonism (Guatteo et al., 2005; Patt et al., 1991; Schulzer et al., 1994). Earlier studies (Verzi et al., 2004; Verzi & Baer, 2005) identified both analytic and numeric equilibria, centers and limit cycles for calcium and stem resistance that coincide with healthy or ailing spine morphologies illustrated in this chapter, and suggested in the literature (Guatteo et al., 2005; Harris, 1999). There are numerous observations about spine loss in the literature (Gerfen, 2006, Patt et al., 1991, and Schulzer et al., 1994), and studies that involve the thermoregulatory role of dopamine within the striata nigra suggest cooling, a reduction in firing frequency, and a decrease in cell input resistance (Brown et al., 1982, Guatteo et al., 2005). The model for calcium and spine morphology uses stem resistance as a measure for cell shape, suggesting long, thin spines under warming conditions and short stubby spines under cooling conditions. One cannot help but wonder what is the morphological precursor to the loss of a dendritic spine? Do spines die as a result of stretching out their stems and increasing input resistance (under cooling and low frequency activation) to the point that the synaptic connection is isolated from the dendrite? Or do they die as a result of being driven down into the dendrite, decreasing input resistance (under warming and high frequency activation) to the point that they can no longer boost or modulate a signal? These are interesting questions that beg more study.

With evidence that ion channel proteins within the dendritic arbor play an important role in thermoregulation (Geffen et al., 1976; Simon, 2006), experimentalists will need to work closely with theoretical biologists to include components within ionic membrane modeling to include dopamine uptake and release, as well as TRPV3 and TRPV4 channel function. Likewise, mathematical modelers need to include components to more accurately capture important dynamics within the striata nigra. A recent Ranvier node model (Smit et al., 2009), based on a modification of the Hodgkin-Huxley model accurately captures excitable membrane properties within the range for human temperatures for large-diameter nerve fibres. Likewise, a model by Moore (1958, as cited in Fitzhugh, 1966) suggests that sodium and potassium conductances (g_{NA} and g_K) in Eq. (5) increase linearly with temperature, where the Hodgkin-Huxley model (1952) assumes they are independent of temperature. Since temperature has been shown to be a significant variable in the study of Parkinson's disease, it may be prudent to multiply these conductances by

$$\eta = A\big[1 + B(T - 6.3)\big], \tag{16}$$

where A is the ratio between ionic conductions of the axon at *6.3 C* and the values used by Hodgkin & Huxley (1952), and B is the rate of change in conductance with temperature, (Fitzhugh, 1966). Measurement data within the striata nigra will be required to accurately fit the parameters A and B. Moreover, with the recent identification of variations in intracellular calcium levels as a contributor to mitochondrial damage (Celci et al, 2009), it is important to include calcium as a component of activity, as well as a consequence. Calcium currents should be included in further theoretical studies to consider the effect of calcium influx to localized cell deterioration.

Patients not adequately controlled with medication may be treated with deep brain stimulation, a current that is thought to block abnormal nerve signals (Benabid, 2003). Other work has demonstrated that high frequency electro-acupuncture stimulation could enhance survival of dopamineric neurons and interfere with abnormal signaling (Jia et al., 2010). These studies suggest that high-frequency stimulation may result in changes in neuronal activity within the basal ganglia, by correcting signal rather than chemical abnormalities. Deep brain stimulation or high frequency electro-acupuncture may induce an inhibitory current, blocking abnormal synaptic activation and excitation (Benabid, 2003, Ascoli et al., 2010). Synaptic inhibition may be thought of as increased membrane permeability to negatively charged ions such as potassium and chloride, which tend to extinguish excitation. Inhibitory conductance in the spine head creates a current path to ground, shunting local currents. For an inhibitory reversal potential, it produces a hyperpolarizing inhibitory postsynaptic potential in the spines. In the presence of synaptic excitation, it reduces the net depolarizing current produced by both the excitatory input and the active channels (Segev & Rall, 1988). Theoretical biologists need to address the connection between deep brain stimulation and Parkinson's disease.

Because a neuron may have as many as ten or twenty thousand spines, small changes in one or more spine parameters could affect the relative weighting of several different synaptic inputs. Nonlinear dynamics in thousands of these compartments along a dynamic geometry within the dendritic arbor may change a single neuron's response to varying input patterns, as well as the dynamic behavior of the entire neuronal subsystem (Segev & Rall, 1988). Severe pathological changes, such as decrease of dendritic length, loss of dendritic spines, and several types of dendritic varicosities have been found in the melanin-containing neurons of substantia nigra pars compacta for Parkinson's patients (Patt et al., 1991). Continuing theoretical studies of action potential generation and propagation under geometric and chemical fluctuations will give insight to the pathology of this complex and devastating disease.

5. Acknowledgments

6. References

Annis, C. M.; O'Dowd, D. K. & Robertson, R. T. (1994). Activity-dependent regulation of dendritic spine density on cortical pyramidal neurons in organotypic slice cultures. *Journal of Neurobiology,* 25(12), (December, 1994), pp. 1483-1493.

Ascoli, G. A.; Gasparini, S., Medinilla, V.; & Migliore, M. (2010). Local control of postinhibitory rebound spiking in CA1 pyramidal neuron dendrites. *Journal of Neuroscience*, 30(18), (May, 2010), pp. 6434-6442.

Basu I., Graupe, D; Tuninetti, D. & Slavin, K. V. (2010). Stochastic modeling of the neuronal activity in the subthalamic nucleus and model parameter identification from Parkinson patient data. *Biological Cybernetics,* 103(6), (June, 2010) pp. 273-283.

Benabid, A. L. (2003). Deep brain stimulation for Parkinson's disease. *Current Opinion in Neurobiology*, 13(6), (December, 2003), pp. 696-706.

Brown, S. J.; Gisolfi, C. V. & Mora, F. (1982). Temperature regulation and dopaminergic systems in the brain: does the substatia nigra play a role? *Brain Research,* 234(2), (February, 1982), pp. 275-286.

Celsi, F.; Pizzo, P.; Brini, M.; Leo, S.; Fotino, C.; Pinton, P. & Rizzuto, R. (2009). Mitochondria, calcium and cell death: a deadly triad in neurodegeneration. *Biochimica, Biophysica Acta.* 1787(5), (May, 2009), pp. 335-344.

Fitzhugh, R. (1966). Theoretical effect of temperature on threshold in the Hodgkin-Huxley nerve model. *General Physiol*ogy, 49(5), (May, 1966), pp. 989-1005.

Geffen, L. B.; Jessell, T. M.; Cuello, A. C.; & Iversen, L. L. (1976). Release of dopamine from dendrites in rat substantia nigra. *Nature,* (March, 1976), 260(3), pp. 258-260.

Gerfen, C. R. (2006). Indirect-pathway neurons lose their spines in Parkinson disease. *Nature Neuroscience,* 9(2), (February, 2006), pp. 157-158.

Guatteo, E.; Chung, K. K.; Bowala, T. K.; Bernardi, G.; Mercuri, N.B. & Lipski, J. J. (2005). Temperature sensitivity of dopaminergic neurons of the substantia nigra pars compacta: involvement of transient receptor potential channels. *Journal of Neurophysiol*ogy, 94(5), (May, 2005), pp. 3069-80.

Harris, K. M. (1999). Calcium from internal stores modifies dendritic spine shape. *Proceedings of the National Academy of Sciences, USA,* 96(22), (October, 1999), pp. 12213-12215.

Hodgkin, A. L. & Huxley, A. F. (1952). A quantitative description of membrane current and its application to conduction and excitation in nerves. *Journal of Physiol*ogy, 117, (March, 1952), pp. 500-544

Jia, J.; Li, B.; Sun, Z. L.; Yu, F.; Wang, X.; & Wang, X. M. (2010). Electro-acupuncture stimulation acts on the basal ganglia output pathway to ameliorate motor impairment in Parkinsonian model rats. *Behavioral Neuroscience*, 124(2), (February, 2010), pp. 305-310.

Patt, S.; Gertz, H. J.; Gerhard, L. & Cervos-Navarro, J. (1991). Pathological changes in dendrities of substantia nigra neurons in Parkinson's diseases: a Golgi study. *Journal of Histology and Histopathology*, 6(3), (July, 1991), pp. 373-380.

Schulzer, M.; Lee, C. S.; Mak, E. K.; Vingerhoets, F. J. G.; & Calne, D. B. (1994). A mathematical model of pathogenesis in idopathic parkinsonism. *Brain,* 117(3), (March, 1994), pp. 509-516.

Segev, I & Rall, W. J. (1988). Computational study of an excitable dendritic spine. *Journal of Neurophysiol*ogy, 60(2), (February, 1988), pp. 499-523.

Simon,   E . (2006). Ion channel proteins in neuronal temperature transduction: from inferences to testable theories of deep body thermosensitivity. *American Journal of Physiology: Regulatory, Integraative and Comparative Physiol*ogy , 291(4), (April, 2006), pp. 273-283.

Smit , J. E.; Hanekom, T.; & Hanekom, J. J. (2009). Modelled temperature-dependent excitability behavior of a generalised human peripheral sensory nerve fibre. *Biological Cybernetics*, 101(7), (July, 2009), pp. 115-`30.

Stephens, B; Mueller, A. J.; Shering, A. F.; Hood, S. H.; Taggart, P.; Arbuthnott, G. W.; Bell, J. E.; Kilford, L; Kingsbury, A. E.; Daniel, S. E.; & Ingham, C. A. (2005). Evidence of a breakdown of corticostriatal connections in Parkinson's disease. *Neuroscience*, 132(3), (March, 2005), pp. 741–754.

Surmeier, D. J.; Guzman, J. N.; Sanchez-Padilla, J. & Goldberg, J. A. (2010). What causes the death of dopaminergic neurons in Parkinson's disease? *Progress in Brain Research,* 183(1), (January, 2010), pp. 59-77.

Verzi, D. W.; Rheuben, M. B. & Baer, S. M. (2004). Impact of time-dependent changes in spine density and spine shape on the input-output properties of a dendritic branch: A computational study. *Journal of Neurophysiology,* 93(12), (December, 2004), pp. 2073-2089.

Verzi, D. W. & Baer, S. M. (2005). Calcium-mediated spine stem restructuring. *Journal of Mathematical and Computer Modelling*, 42(1), (February, 2004), pp. 151-165.

Mechanisms in Parkinson's Disease - Models and Treatments

Edited by Dr. Juliana Dushanova

ISBN 978-953-307-876-2

Hard cover, 582 pages

Publisher InTech

Published online 08, February, 2012

Published in print edition February, 2012

Parkinson's disease (PD) results primarily from the death of dopaminergic neurons in the substantia nigra. Current PD medications treat symptoms; none halt or retard dopaminergic neuron degeneration. The main obstacle to developing neuroprotective therapies is a limited understanding of the key molecular mechanisms that provoke neurodegeneration. The discovery of PD genes has led to the hypothesis that misfolding of proteins and dysfunction of the ubiquitin-proteasome pathway are pivotal to PD pathogenesis. Previously implicated culprits in PD neurodegeneration, mitochondrial dysfunction, and oxidative stress may also act in part by causing the accumulation of misfolded proteins, in addition to producing other deleterious events in dopaminergic neurons. Neurotoxin-based models have been important in elucidating the molecular cascade of cell death in dopaminergic neurons. PD models based on the manipulation of PD genes should prove valuable in elucidating important aspects of the disease, such as selective vulnerability of substantia nigra dopaminergic neurons to the degenerative process.

INTECH
open science | open minds